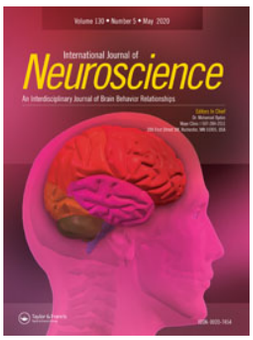

International Journal of Neuroscience

ISSN: 0020-7454 (Print) 1543-5245 (Online) Journal homepage: https://www.tandfonline.com/loi/ines20

Probable role for major facilitator superfamily domain containing 6 (MFSD6) in the brain during variable energy consumption

Sonchita Bagchi, Emelie Perland, Kimia Hosseini, Johanna Lundgren, Noura Al-Walai, Sania Kheder & Robert Fredriksson

To cite this article: Sonchita Bagchi, Emelie Perland, Kimia Hosseini, Johanna Lundgren, Noura Al-Walai, Sania Kheder & Robert Fredriksson (2020) Probable role for major facilitator superfamily domain containing 6 (MFSD6) in the brain during variable energy consumption, International Journal of Neuroscience, 130:5, 476-489, DOI: 10.1080/00207454.2019.1694020

To link to this article: https://doi.org/10.1080/00207454.2019.1694020

Published online: 06 Jan 2020.

INTERNATIONAL JOURNAL OF NEUROSCIENCE
2020, VOL. 130, NO. 5, 476–489
https://doi.org/10.1080/00207454.2019.1694020

Taylor & Francis
Taylor & Francis Group

ORIGINAL ARTICLE

Probable role for major facilitator superfamily domain containing 6 (MFSD6) in the brain during variable energy consumption

Sonchita Bagchi[a], Emelie Perland[a,b], Kimia Hosseini[a], Johanna Lundgren[b], Noura Al-Walai[a], Sania Kheder[b] and Robert Fredriksson[a]

[a]Department of Pharmaceutical Biosciences, Unit of Molecular Neuropharmacology, Uppsala University, Uppsala, Sweden;
[b]Department of Neuroscience, Unit of Functional Pharmacology, Uppsala University, Uppsala, Sweden

ABSTRACT

Purpose: The major facilitator superfamily (MFS) is known as the largest and most diverse superfamily containing human transporters, and these transporters are essential as they sustain the homeostasis within cellular compartments by moving substances over lipid membranes.

Methods: We have identified a novel MFS protein, named Major facilitator superfamily domain containing 6 (MFSD6), and confirmed that it is phylogenetically related to the human Solute Carrier (SLC) transporter family. A homology model of MFSD6 revealed 12 predicted transmembrane segments (TMS) with the classical MFS fold between TMS 6 and 7.

Results: Immunohistological analyses showed specific MFSD6 staining in neurons of wildtype mouse brain tissue, but no expression in astrocytes. Furthermore, we explored expression and probable function(s) of MFSD6 in relation to its phylogenetically related proteins, major facilitator superfamily domain containing 8 (MFSD8) and 10 (MFSD10), which is of interest as both these proteins are involved in diseases.

Conclusions: We showed that expression levels of *Mfsd6* and *Mfsd10* were decreased with elevated or depleted energy consumption, while that of *Mfsd8* remained unaffected.

ARTICLE HISTORY
Received 15 March 2019
Revised 28 September 2019
Accepted 10 November 2019

KEYWORDS
Transporter; energy metabolism; genetics; mRNA; molecular imaging; Major Facilitator Superfamily Domain containing 6 (MFSD6); human Solute Carrier (SLC) transporter family

Introduction

Among the membrane proteins that make up around 27% of all proteins in the human genome [1], the solute carriers (SLCs) are the second largest family with at least 430 [2] members in human. SLC genes encode a wide variety of transporters located in cellular membranes as well as in certain organelle membranes [3]. SLCs are responsible for uptake and flow of several substances including amino acids, nucleotides, sugar, inorganic ions, and drugs across the lipid bilayer. Their diverse substrate specificities indicate several vital functional abilities, such as supply of nutrients, energy production and neurotransmission. SLCs function without direct use of ATP as they move molecules across membranes, against a concentration gradient, either by secondary active transport or by facilitative diffusion [3].

Based on sequence similarity, most mammalian SLC proteins are divided into several protein family (Pfam) clans where the major facilitator superfamily (MFS), amino acid- polyamine organocation (APC), the monovalent cation:proton antiporter (CPA)/anion transporter (AT) and drug/metabolite (DMT) clans contain more than one annotated SLC family [2,4]. Among transporter proteins, MFS is known to be the largest and most diverse superfamily [5,6], with protein homologues in multiple species [7–10]. The MFS superfamily contain transporters that function as uniporters, symporters and antiporters [11], and the human proteins usually possess 12 putative transmembrane segments (TMS) [11,12]. A subgroup of MFS proteins in humans are called Major facilitator superfamily domain containing (MFSD) proteins. They have distinct sequence similarity with SLCs [13] and are referred to as atypical SLCs [2,8].

Here we discern the localisation of MFSD6, one of the 29 novel atypical solute carriers of major facilitator superfamily type [14], showing abundant expression in mouse brain neurons; but not in astrocytes. This is a trait shared by a comparatively well-studied protein, MFSD8 [15, 16]. MFSD8 is expressed at the membrane of lysosomes in human cells [15,16].

CONTACT Sonchita Bagchi Sonchita.Bagchi@farmbio.uu.se Department of Pharmaceutical Bioscience, Unit of Molecular Neuropharmacology, Uppsala University, Uppsala biomedicinska centrum; Box 591, Husargatan 3, 75124 Uppsala, Sweden.
Color versions of one or more of the figures in the article can be found online at www.tandfonline.com/ines.

Mutation in the mouse *Mfsd8* gene provides a reliable animal model for ceroid lipofuscinosis (CLN7) disease [16], strengthening the importance in understanding basic mechanisms involving MFSD proteins. CLN7 is described as a lysosomal disorder [17] and it is an autosomal recessive neurodegenerative disorder with early childhood onset. We confirmed MFSD8 expression by co-localisation of MFSD8 and the lysosomal marker Lamp2. We also showed that MFSD6 is not expressed in the lysosome, even though it has a rather cytosolic expression in both mouse brain tissues and mouse cortex embryonic primary cells. Regarding subcellular localisation, MFSD6 is more similar to another protein from the MFS family, MFSD10 (also known as TETRAN in humans). MFSD10 is not reported to be expressed in lysosome or any other organelle in the cell, but rather located to the plasma membrane [18]. MFSD10 is a protein that transports organic anions in humans [18] and it transports, or causes resistance to, non-steroidal anti-inflammatory drugs (NSAIDs) [19]. Unfortunately, expression of MFSD10 is low in the brain [18], and lack of specific antibody makes it difficult to analyse its localisation at subcellular level. In this study, a detailed phylogenetic analysis showed that MFSD6, MFSD8 and MFSD10 were closely related. Our aim was to determine inter-relation between these three members of the family in terms of localisation and function(s), if any. As MFSDs are known to respond to altered energy intake [9,10,20–22], we also studied whether expressions of *Mfsd6*, *Mfsd8* and *Mfsd10* were affected upon varied food intake (normal chow, 24 h starvation and high-fat diet (HFD). We showed that gene expression of *Mfsd6* and *Mfsd10* were down-regulated in experimental animals exposed toboth the diets, whereas the intracellular *Mfsd8* was primarily unaffected by the difference in diets.

Results

Phylogenetic analysis reveals Mfsd6 to be closely related to Mfsd8 and Mfsd10, as well as to members of some SLC family

Phylogenetic analysis between SLC and MFS family members revealed evolutionary relationships between proteins of these families (Figure 1A). In Figure 1B, 3 major branches have been magnified, where, in one of them, MFSD6 shared branching node with the SLC15 family (A1, A2, A3 and A4) (Figure 1B). Interestingly, it has been shown that, except for SLC15A4, mRNA levels of all SLC15 members are decreased after fasting in Nile tilapia (*Oreochromis niloticus*) while refeeding restores the expression level [23]. Another branching node contained both MFSD8 and MFSD10, which clustered together with SLC46A1 and SLC22A18, suggesting common origin. A previously characterised member of the MFS family, MFSD11 [9], was found within proximity to MFSD6 at the third magnified branch, where it clustered with SLC43 family members (A1, A2 and A3) (Figure 1B). That MFSD6 and MFSD11 were phylogenetically related strengthened the hypothesis of MFSD6 having plausible involvement in energy regulation, since MFSD11 is affected by altered energy homeostasis [9].

The MFSD6, MFSD8 and MFSD10 sequences are conserved in all species analysed

We analysed nine proteomes (*C. elegans*, *D. melanogaster*, *D. rerio, G. gallus*, *H. sapiens*, *M. musculus*, *N. vectensis*, *S. cerevisiae* and *X. laevis)* using Hidden Markov Models (HMM) in order to identify related proteins to human MFSD6, MFSD8 and MFSD10. MFSD6 was identified in all species analysed, except *S. cerevisiae* (labelled green in Figure 2). MFSD8 (blue in Figure 2) and MFSD10 (red in Figure 2) had related proteins in all investigated species, where two larger clusters included all vertebrates. All related proteins were annotated and listed in Table 1. Furthermore, there were proteins identified in the *C. elegans*, *N. vectensis* and *S. cerevisiae* that did not cluster in direct proximity with the human sequences (Figure 2). These proteins were related to MFSD8 and MFSD10, and possibly without specific orthologues in mammals, or that they were more related to proteins not investigated here, such as SLC18A2 in which was identified in the MFSD10 HMM search from zebrafish (Figure 2).

Structural representation of MFSD6, MFSD8 and MFSD10 proteins

We used transmembrane segment (TMS) prediction software 'Protter' [24] (Omasits *et.al.* 2014) that enables interactive protein-feature visualisation and integration with experimental proteomic data, to obtain the TMS characteristics of human MFSD6, MFSD8 and MFSD10. All three proteins had 12 TMS domains with both N and C terminals in intracellular positions. Presence of the classical MFS fold between TMS 6 and 7 (Figure 3A–C) had been detected for all of them as well. MFSD6 had the longest amino acid sequence among the three proteins and it exhibited a relatively long N and C terminal as well as a significant loop between TMS 3 and 4 (Figure 3A).

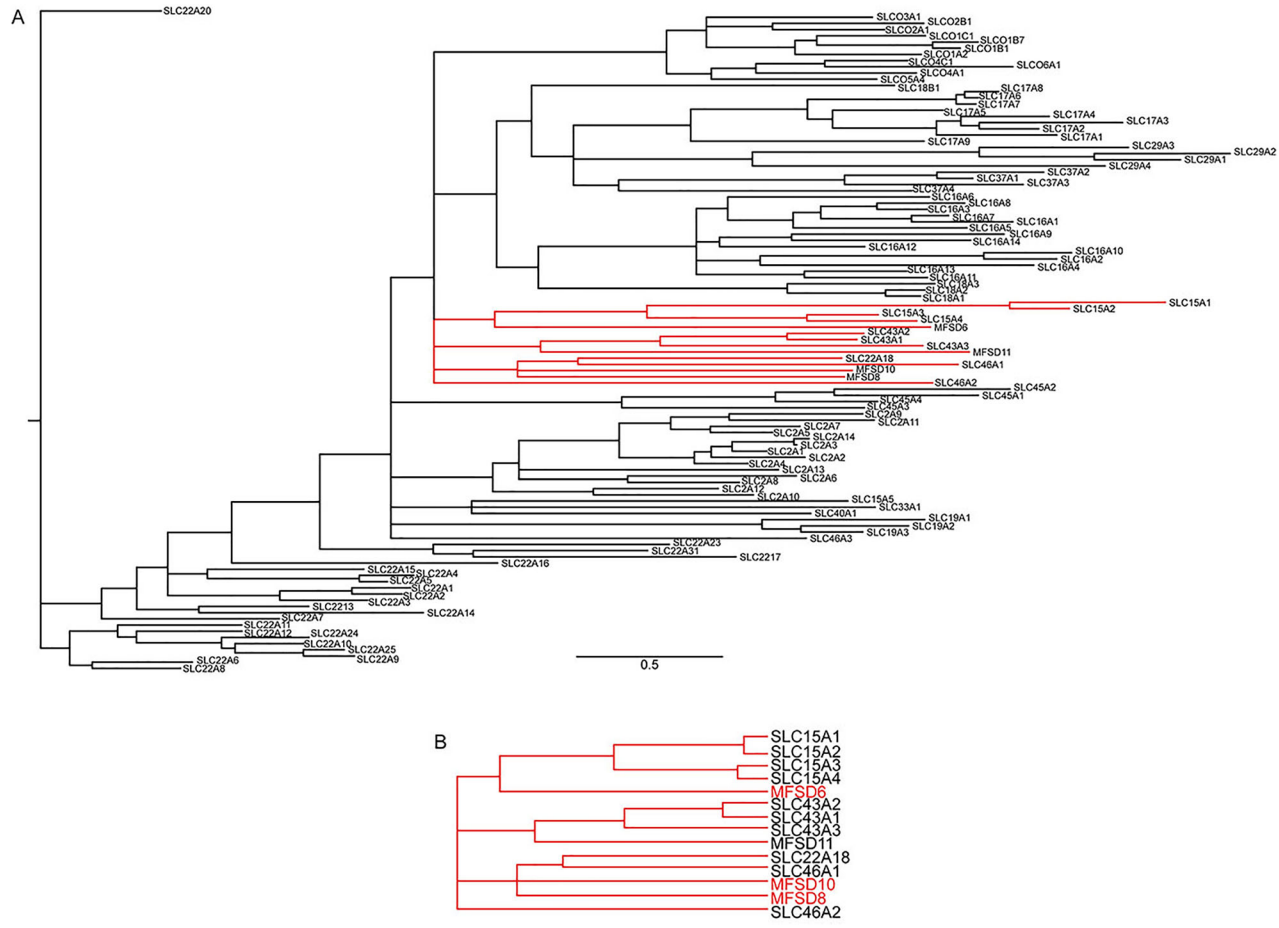

Figure 1. Phylogenetic clustering of MFS and SLC proteins.
(A) A phylogenetic tree is depicted, showing the interrelations between MFSD proteins and all SLCs of MFS type. The highlighted branches include MFSD6 MFSD8, MFSD10 and MFSD11, and are magnified in B. (B) In the zoomed in chart, it is possible to see which SLCs that are most closely related to MFSD6, MFSD8 and MFSD10.

Predicted 3 D structures of MFSD6, MFSD8 and MFSD10

12 possible TMS for MFSD6 (Figure 3D), MFSD8 (Figure 3E) and MFSD10 (Figure 3F) were also identified when building homology models, using SWISS-MODEL [25]. The protein sequences were aligned against a structurally known MFS protein template [26], where the MFSD6 model had global model quality estimation (GMQE) value of 0.27, the MFSD8 model had 0.44 and MFSD10 had 0.5. GMQE scale range from 0 to 1, where higher numbers indicate a better model. The tertiary structures from top view indicated formation of a pore, through which a substrate possibly could be transported in MFSD6 (Figure 3G), MFSD8 (Figure 3H) and MFSD10 (Figure 3I). Both N and C terminals were located in the cytoplasm for all three proteins. They also exhibited the classical MFS fold between TMS 6 and 7. Unlike MFSD8 and MFSD10, MFSD6 contained a long hydrophilic loop between TMS 3 and 4 (Figure 3D).

mRNA expression patterns of Mfsd6, Mfsd8 and Mfsd10 in normal mouse tissue displays abundant distribution

RNA from blood and several tissues (brain stem, cerebellum, cortex, eye, heart, hippocampus, hypothalamus, intestine, kidney, liver, lungs, olfactory bulb, ovary, spinal cord, spleen, striatum, thalamus, thymus and uterus) from wild-type mice were extracted. Then qRT-PCRs were run on the samples using specific primers for *Mfsd6*, *Mfsd8* and *Mfsd10* followed by normalisation against the geometric mean of five stable housekeeping genes, *Gapdh, β-tubulin, Rpl19, Cyclo* and *Actin b*. *Mfsd6* (Figure 4A), *Mfsd8* (Figure 4B) and *Mfsd10* (Figure 4C) were expressed in both central and peripheral tissues, as depicted in the graphs.

Western blot analysis with MFSD6-targeted SiRNA knocked down cells validates specificity of MFSD6 antibody

To ascertain the specificity of the commercially bought anti-MFSD6 antibody, western blot was run on both wildtype and

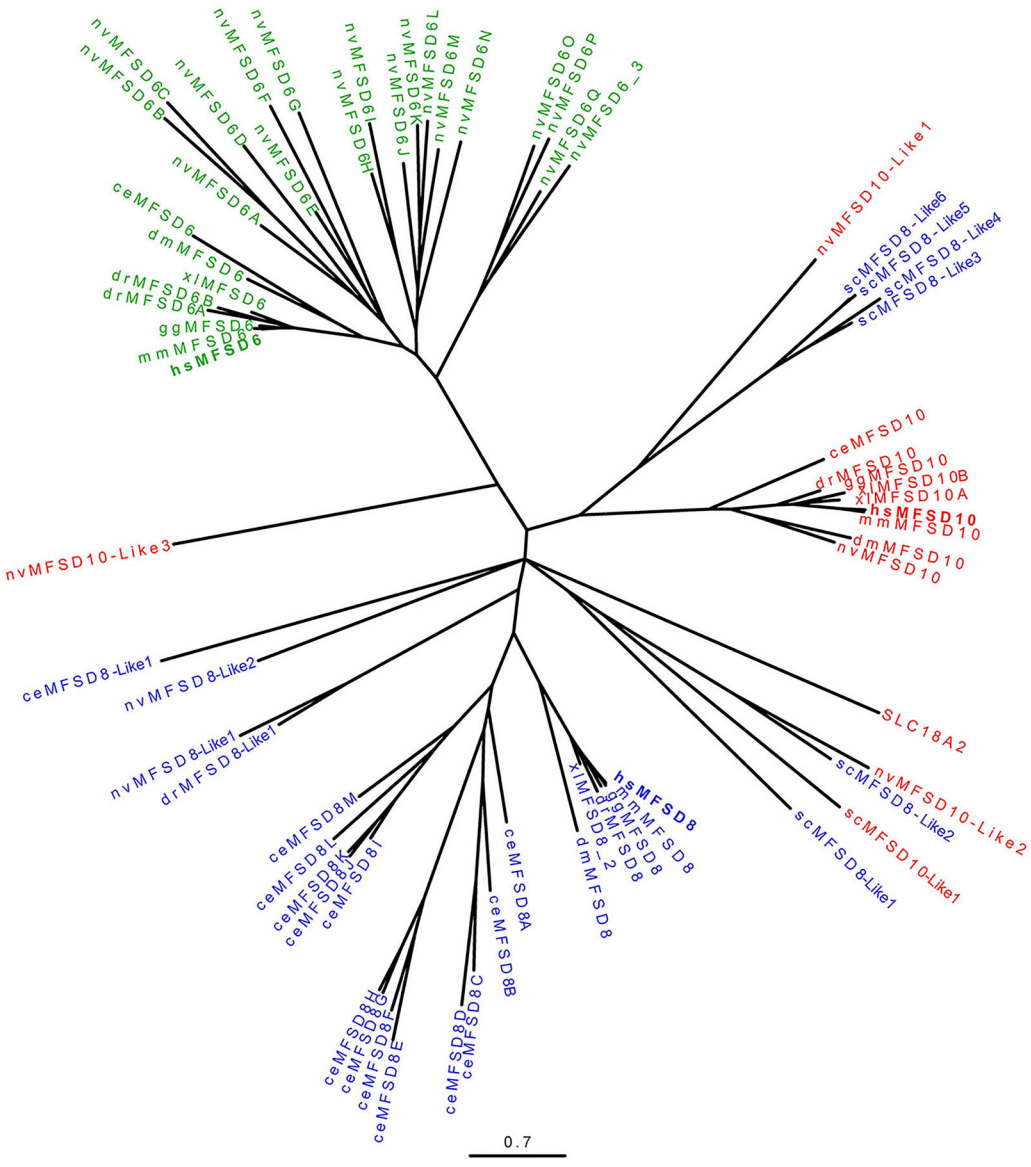

Figure 2. Identification of related proteins in various species.
Hidden Markov Models are built for MFSD6, MFSD8 and MFSD10, and used to search several proteomes for relative proteins. Their interrelationships are inferred in the depicted tree. Green colored entries represent MFSD6 related proteins whereas blue is MFSD8 and red is MFSD10 related proteins. Abbreviations: ce, *Caenorhabditis elegans*; dm, *Drosophila melanogaster*; dr, *Danio rerio*; gg, *Gallus gallus*; hs, *Homo sapiens*; mm, *Mus musculus*; nv, *Nematostella vectensis*; sc, *Saccharomyces cerevisiae;* xl, *Xenopus laevis*. See Table 1 for detailed information about each protein.

knocked down PC12 cells with MFSD-targeted SiRNA. The western blot resulted in one band at 55 kDA (Figure 5A), which corresponded well with the size of the annotated mouse splice variants in C57BL6 mice, with predicted protein size 63kDA (ENSEMBL transcript ENSMUST00000147758.7; Ensembl version 86). The size of the band detected was within ±10kDA from the predicted sizes, which suggested that the antibody was detecting MFSD6. To confirm its specificity further, MFSD-targeted SiRNA was used on PC12 cells to knock down the expression of MFSD6 and the expression intensity was compared with that of wildtype PC12 cells, as well as with that of cells transfected with non-specific SiRNA. 16% reduction in relative density was recorded in comparison with the PC12 wildtype control (Figure 5B).

MFSD6 is expressed in excitatory neurons, but not in the astrocytes of mouse wildtype brain tissue sections

Specific antibodies for MFSD6 protein in reference to different neural markers (refer to Table 2 for concentrations of individual antibodies) were used to study its subcellular localisation. The markers used were NeuN for Neuronal cells [27], glutaminase marker PAG for excitatory neurons [28,29] and GFAP for astrocytes [30]. MFSD6 was stained in neuronal cells (Figure 6A) and more specifically in glutaminase positive cells (Figure 6B), but not in astrocytes (Figure 6C). To compare subcellular localisation of MFSD6 with that of MFSD8, similar double immuno-histochemical

Table 1. Annotation of MFSD6, MFSD8 and MFSD10 related proteins.

	MFSD6		MFSD8		MFSD10	
Species	Annotated name	Accession number	Annotated name	Accession number	Annotated name	Accession number
African clawed frog	MFSD6	XP_018092375.1	MFSD8	NP_001085636.1	MFSD10A	NP_001084807.1
					MFSD10B	NP_001088384.1
Chicken	MFSD6	XP_421837.1	MFSD8	XP_420463.1	MFSD10	XP_015141347.1
C. elegans	MFSD6	NP_498662.1	MFSD8A	NP_001022903.1	MFSD10	NP_510814.1
			MFSD8B	NP_509296.1		
			MFSD8C	NP_505586.1		
			MFSD8D	NP_001256536.2		
			MFSD8E	NP_503058.1		
			MFSD8F	NP_504616.1		
			MFSD8G	NP_001263885.1		
			MFSD8H	NP_501823.2		
			MFSD8I	NP_505957.1		
			MFSD8J	NP_496546.2		
			MFSD8K	NP_503443.1		
			MFSD8L	NP_505341.1		
			MFSD8M	NP_505338.1		
			MFSD8-Like1	NP_505506.2		
Fruit fly	MFSD6/Jet fuel	NP_610983.1	MFSD8	NP_648107.3	MFSD10	NP_524429.1
Mouse	MFSD6	NP_598590.2	MFSD8	NP_082416.2	MFSD10	NP_080936.1
Starlet sea anemone	MFSD6A	XP_001641011.1	MFSD8-Like1	XP_001641823.1	MFSD10	XP_001641315.1
	MFSD6B	XP_001623781.1	MFSD8-Like2	XP_001638874.1	MFSD10-Like1	XP_001631992.1
	MFSD6C	XP_001639031.1			MFSD10-Like2	XP_001638965.1
	MFSD6D	XP_001641131.1.1			MFSD10-Like3	XP_001636386.1
	MFSD6E	XP_001629670.1				
	MFSD6F	XP_001641130.1				
	MFSD6G	XP_001635934.1				
	MFSD6H	XP_001629902.1				
	MFSD6I	XP_001638755.1				
	MFSD6J	XP_001634979.1				
	MFSD6K	XP_001629466.1				
	MFSD6L	XP_001635035.1				
	MFSD6M	XP_001634981.1				
	MFSD6N	XP_001626053.1				
	MFSD6O	XP_001638321.1				
	MFSD6P	XP_001639123.1				
	MFSD6Q	XP_001625307.1				
	MFSD6R	XP_001630859.1				
Zebrafish	MFSD6A	NP_001076525.1	MFSD8	NP_001038513.1	MFSD10	NP_001017667.1
	MFSD6B	NP_001315145.1	MFSD8-Like1	XP_009295888.1	SLC18A2	AAH90766.1
Yeast			MFSD8-Like1	EIF49876.1	MFSD10-Like1	EGA77103.1
			MFSD8-Like2	EJT43793.1		
			MFSD8-Like3	EGA63184.1		
			MFSD8-Like4	XP_020063523.1		
			MFSD8-Like5	XP_002416836.1		
			MFSD8-Like6	XP_003868136.1		

experiments with the same markers were run for MFSD8 and MFSD10. Like MFSD8, MFSD6 stained the neuronal cells (Figure 6D), specifically the glutaminase positive cells (Figure 6E), but not the astrocytes (Figure 6F). Unfortunately, due to low expression of MFSD10 in brain tissue, we did not observe any prominent staining in our experiments (data not shown).

Fluorescent immunocytochemistry on embryonic primary cortex cells show no expression of MFSD6 in lysosomes, unlike MFSD8

Co-staining of MFSD6 and MFSD8 with PAN showed their neuronal expressions (Figure 7A–H). MFSD6 (Figure 7A) was co-stained with PAN (Figure 7B) and the nuclear marker DAPI (Figure 7C), as seen in the merged image (Figure 7D), confirmed neuronal localisation of the protein. Similarly, MFSD8 (Figure 7E) and PAN (Figure 7F) together with DAPI (Figure 7G) co-localised in the merged image (Figure 7H). However, no overlap in staining was observed at the merged image between MFSD6 and the lysosomal marker Lamp2 [31] (Figure 7I) together with DAPI, suggesting no expression of MFSD6 in the lysosomes. On the other hand, in the merged image between MFSD8 and Lamp2 (Figure 7J), there was co-localisation confirming the lysosomal localisation of MFSD8.

Gene expression of Mfsd6 and Mfsd10 is downregulated at both levels of energy consumption, while that of Mfsd8 remains stable

The qRT-PCRs illustrated that gene expression of *Mfsd6* and *Mfsd10* were reduced as energy intake of

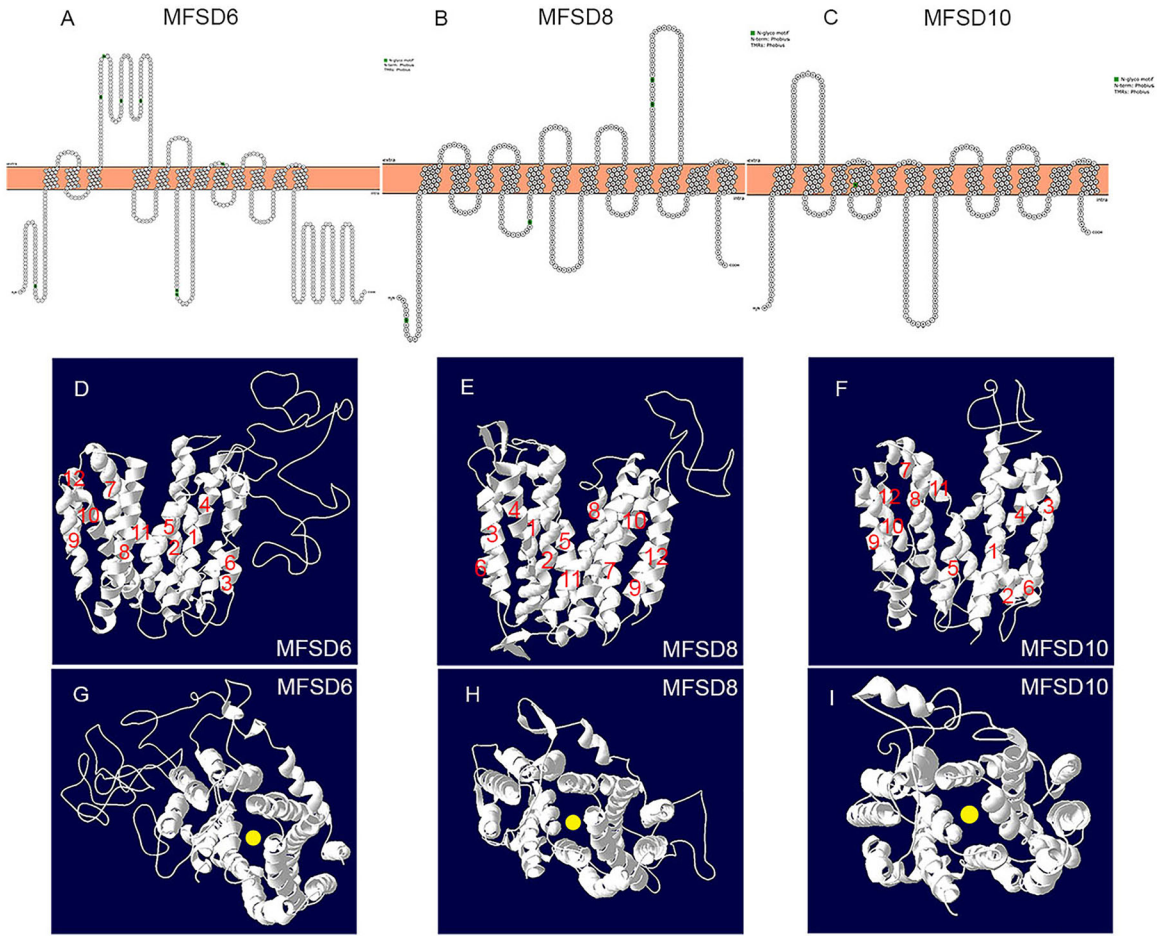

Figure 3. Predicted structures of human MFSD6, MFSD8 and MFSD10.
Topology prediction of the human (A) MFSD6, (B) MFSD8 and (C) MFSD10 proteins are used to visualise the transmembrane segments. Predicted 3D structures of (D) MFSD6, (E) MFSD8 and (F) MFSD10 are obtained using the Swiss-Model, where MFS proteins are used as templates. The top-view of proteins (G) MFSD6, (H) MFSD8 and (I) MFSD10 exhibit a possible substrate pore (marked in yellow) for each protein.

the animals changed by variable diet. Mice on normal chow were used as controls and the data obtained was compared with mice that were starved for 24 h as well as mice fed HFD for eight weeks. Brains from each category were cut into 7 coronal sections (Figure 8A), image adapted from [9], and changes in their gene expression were recorded by qRT-PCR. *Mfsd6* was significantly increased in section 1 ($p = 0.0073$) and reduced in section 2 ($p = 0.0006$), section 3 ($p = 0.0106$) and section 7 ($p = 0.0181$) after starvation. Also, HFD decreased the expression levels with the following significance values: section 2 ($p = 0.0029$), section 3 ($p \leq 0.0001$), section 4 ($p = 0.0097$), section 5 ($p = 0.0021$), section 6 ($p = 0.0084$) and section 7 ($p = 0.018$) (Figure 8B). *Mfsd8* was more stable and up-regulated in section 1 ($p = 0.0423$), while down-regulated in section 2 ($p = 0.0025$) and section 6 ($p = 0.0469$) after starvation. After HFD, *Mfsd8* was only up-regulated in section 1 ($p = 0.039$) (Figure 8C), which includes only the olfactory bulb, and this will not be discussed any further. Finally, *Mfsd10* was altered by both diets where starvation resulted in down-regulated expression in section 2 ($p = 0.002$), section 3 ($p = 0.0014$) and section 5 ($p = 0.016$) (Figure 8D). HFD reduced *Mfsd10* ubiquitously in the brain (Figure 8D); section 1 ($p = 0.048$), section 2 ($p = 0.0061$), section 3 ($p < 0.0001$), section 4 ($p = 0.0004$), section 5 ($p < 0.0001$), section 6 ($p = 0.041$) and section 7 ($p = 0.0091$).

Discussion

MFSD6 in humans is identified as an orphan member of the large MFS clan [2]. Here we show that expression of MFSD6 and MFSD10 changes at the mRNA level in response to energy status, suggesting that these two transporters have a role in regulation of energy homeostasis.

We used a mouse mRNA panel [9] to study the global expressions of *Mfsd6*, *Mfsd8* and *Mfsd10* in the brain and periphery. All three genes were abundantly expressed in the mouse; *Mfsd6* displayed

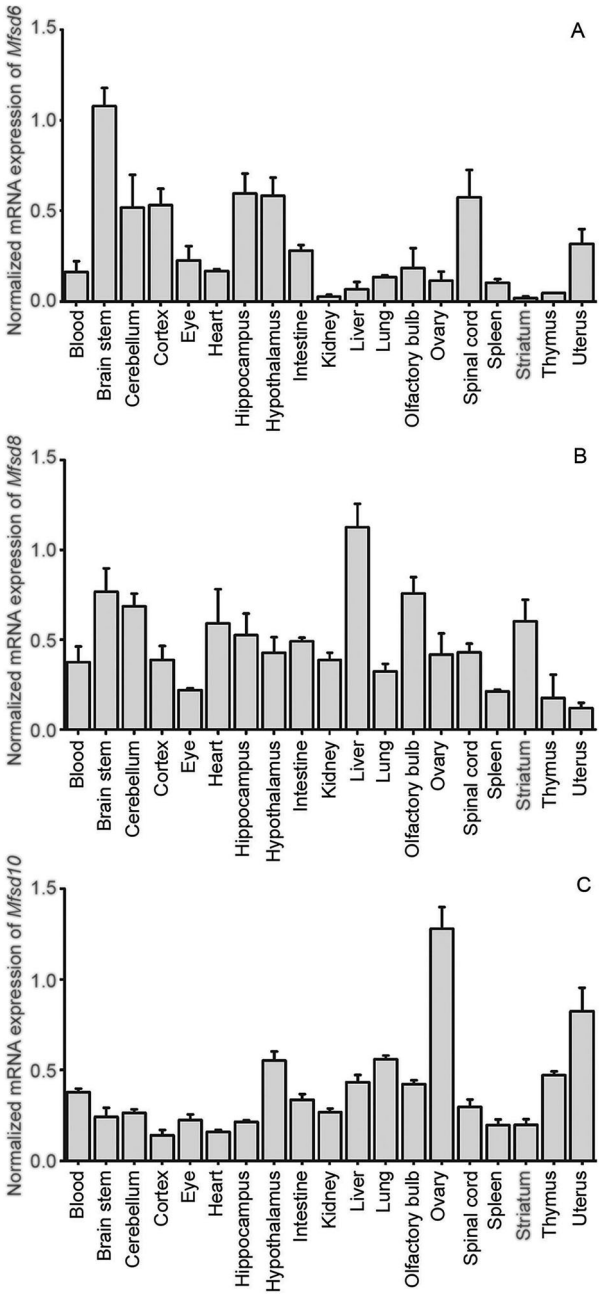

Figure 4. Abundant Mfsd6, Mfsd8 and Mfsd10 gene expressions.

The column charts display the normalised relative mRNA expression levels (±SD) of (A) *Mfsd6*, (B) *Mfsd8* and (C) *Mfsd10* throughout a mouse. The expressions are normalised against the geometric mean of five stable housekeeping genes, *Gapdh*, *β-tubulin*, *Rpl19*, *Cyclo* and *Actin b*. All genes display abundant expression and are found throughout the mouse body. However, *Mfsd6* has slightly higher relative expression in central than the peripheral regions (A) whereas *Mfsd8* expression varies throughout the body (B) and *Mfsd10* has a homogenous pattern (C).

relatively higher expression levels in central areas compared to the periphery whereas *Mfsd8* and *Mfsd10* had more homogenous levels. So even if these genes had common evolutionary origin (Figure 1A and B), they diverged from each other in their expression map.

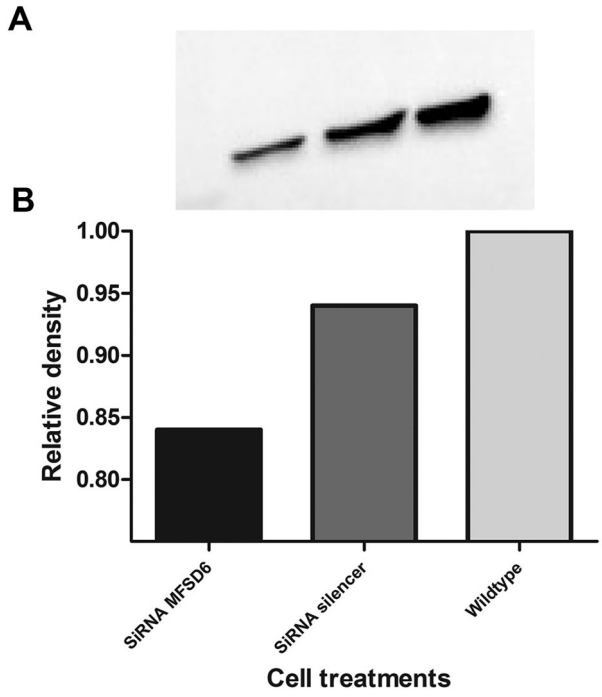

Figure 5. Western blot analysis on PC12 cells to validate MFSD6 antibody.

(A) Western blot analysis shows one clear band (55 kDA) indicating the detection of MFSD6 antibody. (B) Furthermore, MFSD6 specific SiRNA was used to knock down the protein in PC12 cells and the relative density of expression was compared with wildtype PC12 cells. 16% reduction in relative density of the bands of the western blot confirms validation of MFSD6 antibody. An extra control was run by treating PC12 cells with unspecific SiRNA (silencer).

Immunohistological staining on wildtype mouse brain tissue showed that all three proteins were expressed in neuronal cells, but not in astrocytes. This suggests that MFSD6, MFSD8 and MFSD10 could have similar regulation pathways and that there could even be cross-talk between them. Hence, it would be of interest to study their interactions and/or relationships further by knocking one of the proteins down with specific SiRNA and measuring any alteration in gene expression of the other two *Mfsd*s in immortal cell lines and embryonic primary cortex cell cultures. We detected low expression of MFSD10 staining in tissue from wildtype mouse brain while no staining in the embryonic primary cortex cells was observed. This indicates that MFSD10 either is not expressed at early embryonic stage and that it is developed later on after birth or it is not expressed in cortex where the embryonic primary cells were collected from.

We used C57BL6/J mice to study involvement of *Mfsd6*, *Mfsd8* and *Mfsd10* in energy homeostasis *in vivo*. Interestingly, the expression of *Mfsd6* and *Mfsd10* was significantly down-regulated between bothconditions, while *Mfsd8* expression levels were more stable throughout the experiment. This result could depend

Table 2. Details of antibodies used for fluorescent immunohistochemistry and immunocytochemistry.

Primary antibodies	Species	Dilution	Company	Catalogue number
Anti-MFSD6	Goat	1:20	Sigma-Aldrich SAB2502050	
Anti-MFSD8	Rabbit	1:50	Sigma-Aldrich HPA044802	
Anti-MFSD10	Rabbit	1:20	Sigma-Aldrich HPA037398	
Anti-NeuN	Mouse	1:400	Millipore MAB377	
Anti-GFAP	Mouse	1:400	Millipore MAB360	
Anti-glutaminase	Mouse	1:100	AbCam ab60709	
Anti-PAN	Mouse	1:300	Millipore MAB2300	
Anti-Lamp2	Rat	1:100	Abcam ab13524	
Secondary antibodies	**Species**	**Dilution**	**Company**	
Anti-rabbit-594	Donkey	1:400	Thermo Fisher Scientific A21207	
Anti-rabbit-488	Donkey	1:400	Thermo Fisher Scientific A21206	
Anti-goat-488	Donkey	1:400	Thermo Fisher Scientific A11055	
Anti-mouse-488	Donkey	1:400	Thermo Fisher Scientific A21202	
Anti-rat-594	Donkey	1:400	Thermo Fisher Scientific A21209	
Anti-rat-488	Donkey	1:400	Thermo Fisher Scientific A21208	
Anti-mouse-594	Goat	1:400	Thermo Fisher Scientific A11005	
Anti-mouse-488	Goat	1:400	Thermo Fisher Scientific A11029	
Anti-rat-488	Goat	1:400	Thermo Fisher Scientific A11006	

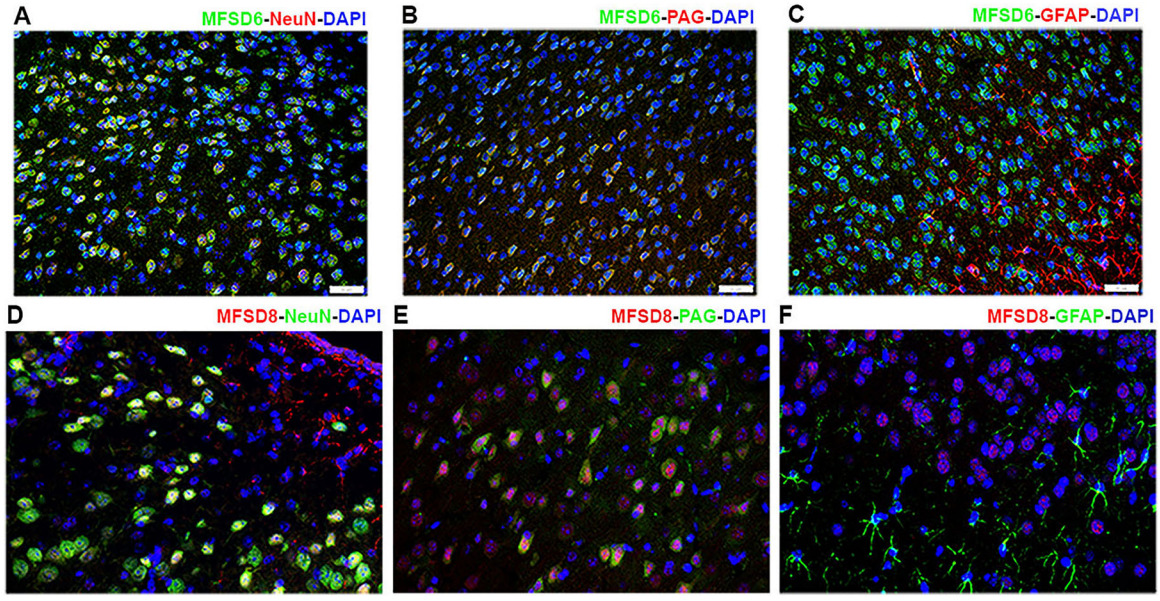

Figure 6. Neuronal expression of MFSD6 and MFSD8 in mouse brain.
(A–F) Fluorescent immunohistochemistry staining on coronal mouse brain sections displays MFSD6 and MFSD8 expressions in neurons. (A) Double immunostaining with MFSD6 (green) and NeuN (red) gives rise to the merged image of MFSD6 in mouse brain where the nucleuses were stained with DAPI (blue). (B) Double immunostaining with MFSD6 (green) and PAG (red) gives rise to the merged image of MFSD6 in mouse brain where the nucleuses were stained with DAPI (blue). (C) Double immunostaining with MFSD6 (green) and GFAP (red) gives rise to the merged image of MFSD6 in mouse brain where the nucleuses were stained with DAPI (blue). Merged micrographs of double immunohistochemistry illustrate localisations of (D) MFSD8 (red) and NeuN (green), (E) MFSD8 (red) and PAG (green), (F) MFSD8 (red) and GFAP (green). The nuclei are stained with DAPI in blue in all images. The merged images display overlay between the neuronal marker NeuN and both MFSD6 (A) and MFSD8 (D) as well as between the glutaminase marker PAG and both MFSD6 (B) and MFSD8 (E), but no co-staining between either of them and the glial cell marker GFAP (C and F).

on their subcellular location; that MFSD6 and MFSD10 are expressed in the plasma membrane [18] and/or in the cytosol, whereas MFSD8 is in the lysosomes [15]. That MFSD6 and MFSD10 could be located to the plasma membrane suggests that they are more susceptible toward concentration changes in the body, and their expressions would be more easily adjusted. Since it has been shown in cell lines that lysosomes stabilise within 12 h of starvation [32], it is possible that similar effects occur *in vivo*, which could explain stable *Mfsd8* levels. It could also be that 24 h starvation is a rather short time in mice, and that the extracellular nutrient changes have not exceeded into the cell yet, as the transporters on the plasma membrane has been adjusted accordingly. This means that the intracellular environment would be unchanged, so that there would be no reason for the cell to adjust the lysosomal *Mfsd8* levels. On the other hand, *Mfsd6* and *Mfsd10* were downregulated even after 24 h, possibly through the multivesicular body (MVB) pathway, which is the primary means of degradation of transmembrane proteins in response to nutrient stress [33]. C57BL6 mice are

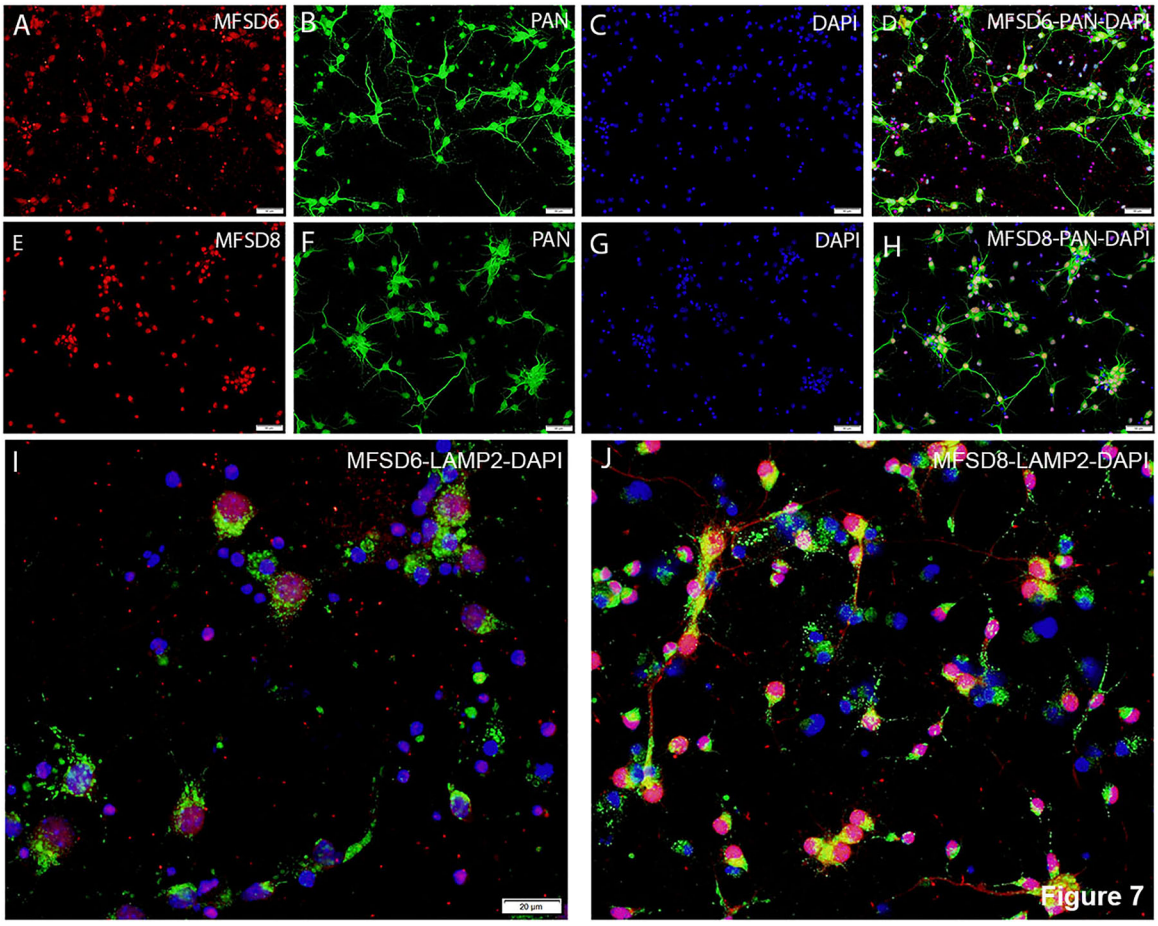

Figure 7. Subcellular localisation of MFSD6 and MFSD8.
Fluorescent immunocytochemistry on embryonic primary cortex cells shows neuronal expression of both MFSD6 and MFSD8. However, unlike MFSD8, no expression of MFSD6 is detected in lysosomes. (A) Staining with MFSD6 antibody. (B) Staining of the same cells with PAN. (C) Staining of the same cells with DAPI. (D) Merged image showing co-localisation of MFSD6, PAN and DAPI. (E) Staining with MFSD8 antibody. (F) Staining of the same cells with PAN. (G) Staining of the same cells with DAPI. (H) Merged image showing co-localisation of MFSD8, PAN and DAPI. (I) Merged image of MFSD6 immunostaining with lysosomal marker Lamp2 and DAPI, showing no overlap between immunocytochemistry of MFSD6 and Lamp2. (J) Merged image of MFSD8 immunostaining with lysosomal marker Lamp2 and DAPI, confirming co-localisation between MFSD8 and Lamp2.

also known to obtain the metabolic syndrome when changing diets [34], so effects seen can also be due to other confounding factors. However, we find it most likely that they are direct effects of nutritional status.

Taken everything together, this work can be used as base on which further work can be built. This study showed results indicating a possible role of MFSD6 in energy homeostasis. Additionally, we found MFSD6 to be a very interesting target due to its relationship to MFSD8 and MFSD10, two proteins known to be involved in human diseases and pharmacology. It will be very interesting to see what function(s) MFSD6 have, what system(s) it is involved in and with what other proteins it interacts with.

Experimental procedures

Phylogenetic analysis

Human SLC amino acid sequences of MFS type [2] and certain human proteins including MFS motifs (MFSD6, MFSD8, and MFSD10 and MFSD11) were downloaded from Ensembl release 84 [35]. The phylogenetic relationships between the sequences were inferred as described in [10]. Briefly, Bayesian approach was used as implemented in mrBayes 3.2.2 [36, 37] to obtain the chart. It was run on six chains (five heated and one cold) with two runs in parallel (n runs = 2) under the mixed amino acid model with eight gamma categories and invgamma as gamma rates for a maximum of 2,000,000 generations. The final tree was calculated using the best 75% of all generated trees.

Hidden Markov Models (HMM) were built for MFSD6, MFSD8 and MFSD10, using HMMbuild from the HMMER package (Eddy, 2011). Then several data sets (*C. elegans*, *D. melanogaster*, *D. rerio, G. gallus*, *H. sapiens*, *M. musculus*, *N. vectensis*, *S. cerevisiae* and *X. laevis*), obtained from Ensembl [35], were scanned in search for orthologues to the human proteins. The results were manually curated, and splice variants and

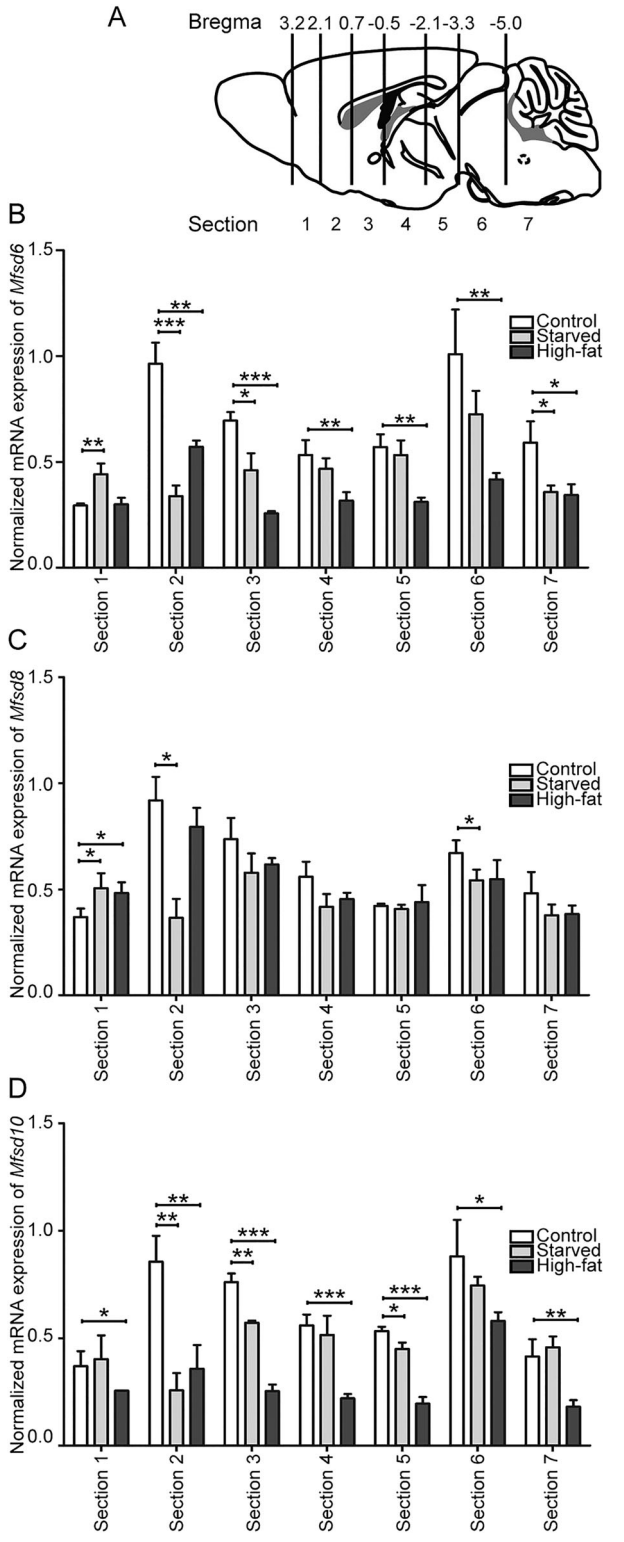

Figure 8. Altered food intake affects transcription levels of Mfsd6 and Mfsd10.

Mice were divided into three groups based on food intake: 1) normal food, considered as controls, 2) 24h starvation and 3) high-fat diet, and the brains were cut into (A) 7 coronal sections according to [9]. Normalised relative mRNA levels (±SD) are plotted after qRT-PCR analyses using the brain sections of three groups described above. Normalisation is made using three stable housekeeping genes, *Gapdh*, *H3a* and *Actinb*. Unpaired t-tests, followed by Bonferroni correction for multiple testing; significance levels are set to $*p < 0.0493$, $**p < 0.00998$, $***p < 0.001$. The relative expression of (B) *Mfsd6*, (C) *Mfsd8* and (D) *Mfsd10* in the 7 brain areas are depicted in the graphs.

pseudogenes were removed. Protein sequences were aligned using multiple PSI/TM tcoffee sequence alignment [38]. The protein-interrelations were analysed in a phylogenetic tree, as described above.

Sequence and homology modelling

The transmembrane (TM) prediction software 'Protter' [24] was used for interactive protein feature visualisation and integration with experimental proteomic data to obtain the protein topology of human MFSD6, MFSD8 and MFSD10. The fully automated homology Swiss-Model program [25] was used to build 3 D models, where MFS transporters were used as templates. A structurally known MFS transporter protein found in several gram-negative bacteria, YajR, [26] was used as template for the MFSD6, MFSD8 and MFSD10 models, providing GMQE scores at 27, 44 and 50 respectively. Manual inspections of the alignments were performed to verify that conserved MFS motifs, such as the MFS fold [39] were aligned to enhance credibility of the models. Tertiary structures were finalised using Swiss-Pdb Viewer [40] and Adobe Photoshop CS6.

Animals

All procedures involving mice were approved by the local ethical committee in Uppsala (Permit Number C39/16, C419/12 and C67/13), and in unity with the EU-directive 2010/63. All animals had free access to food and water at all times unless anything else is stated. They were kept under a 12 h light-dark cycle and euthanised during the light period. C57BL6/J mice (Taconic M&B, Denmark) were used in all trials.

Sample collection for mouse RNA panel

Wildtype male mice were used to isolate central and peripheral tissues, while females were euthanised for female genitalia ($n = 5$ per organ). Mice were sacrificed by cervical dislocation and all dissections were performed on ice within 10 min after utilisation. Tissues were kept in RNA-later (Qiagen) at room temperature for 2 h before freezing at -80 °C. Blood was collected *via* a cardiac puncture after utilising the animal. The blood was mixed with EDTA (1.5 mg/ml blood, VWR) and centrifuged for 10 min at 4 °C at maximum speed of 21100 $\times g$. Then the pellet was used for RNA extraction.

RNA extraction and cDNA synthesis

Absolutely RNA Miniprep Kit (Agilent Technologies) was used to extract RNA from individual samples according to manufactures description and a detailed description can be read at [9]. Briefly, tissues were homogenised using a Bullet blender, followed by centrifugation (Heraesus Fresco 21 centrifuge) of the samples through various spin-cups to remove cell debris, RNA precipitation and finally elution. Concentration was measured using ND-1000 spectrophotometer (NanoDrop Technologies).

1 μg extracted RNA was subsequently used as template for the cDNA synthesis. The High Capacity RNA-to-CDNA kit (Invitrogen) was used according to manufactures instructions. The RNA was added to 2RT Reaction mix and RT enzyme mix and the final volume was adjusted to 20 μL with DEPC-treated water before following cDNA synthesis cycle; 10 min incubation at 25 °C, then 30 min at 50 °C before terminating the reaction at 85 °C for 5 min. Samples were cooled before 2 U E.coli RNase H was added and additional 20 min incubation at 37 °C was performed. cDNA from the same organ, but from different animals, were pooled and diluted to 5 ng/μl RNA in sterile water.

Primer design and quantitative real-time PCR

All primers were designed using Beacon Design 8 (Premier Biosoft, Palo Alto, CA, USA). Samples were amplified using the following primers: *Mfsd6* forward 5′-caactcaccagattccta -3′ and reverse 5′-cctacttactccttcacaa -3′, *Mfsd8* forward 5′-attctaatactgccattca-3′ and reverse 5′-ctatacctcttacttcactt-3′and *Mfsd10* forward 5′-cctgtctg tggaaatggt-3′ and reverse 5′-cagtgtctctggcaagaa-3′. Six housekeeping genes were run: glyceraldehyde-3-phosphate dehydrogenase (*Gapdh*) forward 5′-gccttccgtgt tcctacc-3′, reverse 5′-gcctgcttcaccaccttc-3′, beta tubulin 4B (*bTub*) forward 5′-agtgctcctcttctacag-3′, reverse 5′-tatctccgtggtaagtgc-3′, ribosomal protein L19 (*Rpl19*) forward 5′-aatcgccaatgccaactc-3′, reverse 5′-ggaatggacagtcacagg-3′, histone cluster 1 (*H3a*) forward 5′-ccttgt gggtctgtttga-3′, reverse 5′-cagttggatgtccttggg-3′, peptidylpropyl isomeras A (*Cyclo*) forward 5′-tttgggaaggtgaa agaagg-3′, reverse 5′-acagaaggaatggtttgatgg-3′ and actin-related protein 1B (*Actb*) forward 5′-ccttcttgggtatgg aatcctgtg-3′, reverse 5′-cagcactgtgttggcatagagg-3′.

For the quantitative real-time (qRT-PCR) reaction; 5 ng/μl RNA pooled cDNA, 0.05 μl of each primer (100 pmol/μl), 3.6 μl 2x reaction buffer including 20 mM $MgCl_2$ (Thermo scientific), 0.2 μl of 25 mM dNTP mix (Fermentas), 1 μl DMSO, 0.5 μl of SYBR Green (1:50000; Invitrogen) in TE buffer (pH 7.8) and 0.08 μl of DreamTaq polymerase (Thermo scientific) was mixed. The amplification was done using an iCycler real-time detection instrument (Bio-Rad Laboratories) where the reaction conditions were: initial denaturation for 30 sec at 95 °C followed by 45 cycles of 10 sec at 95 °C, 30 sec at 55-61 °C (optimal temperature for each primer pair) and 30 sec at 72 °C. A melting curve was performed by 81 cycles of 10 sec each, starting at 55 °C with an increase of 0.5 °C per cycle. All reactions were performed in triplicates on each plate, and each plate was repeated twice. Negative controls were included on each plate.

Analysis of wildtype mouse qRT-PCR panel

CT-values were collected using MyIQ software (Bio-Rad Laboratories) followed by primer efficiency calculations using LinRegPCR software. Grubbs test (GraphPad software) was run to remove outliers in the primer efficiency calculation before normalising the values by using the GeNorm [41]. Stable housekeeping genes were identified (*Gapdh*, *bTub*, *Rpl19*, *Cyclo* and *Actb*) and their geometric means were used as normalisation factors for each tissue. Normalised relative mRNA levels (±SD) were plotted in the charts.

Knock down of MFSD6 by SiRNA

The day before transfection, PC12 cells (ATCC, USA) were seeded on 6 well plates (Thermofisher, Uppsala, Sweden) to obtain 80% confluency. On the day of transfection, 9ul/well RNAiMAX reagent (Thermofisher) was diluted with 150ul/well Opti-MEM (Thermofisher) to prepare diluted lipofectamine. SiRNA Silencer select MFSD6 (30 pmol) (Ambition, USA) and SiRNA Silencer negative control (30 pmol) (Ambition, USA) were also diluted separately in 150ul/well Opti-MEM medium at the ratio of 1:1. Respective diluted siRNA were then added to diluted lipofetamine-RNAiMAX mix and incubated for 5 min at room temperature. 250ul/well of siRNA-lipid complex were added to the cells. One or two wells of the same plate containing same confluency of cells were treated only with diluted lipofectamine-RNAiMAX reagent and used as wildtype control. The plate was incubated in the 37 °C incubator. After 2 days cells were washed twice with 1 ml/well cold PBS, lysed using 300ul/well ice-cold Pierce RIPA buffer (Thermofisher) and collected in 1 ml microcentrifuge tubes. They were then centrifuged at 14000 g for 15 min. Supernatant were carefully collected and stored in -80 freezers, if not used immediately. Western blot was performed using anti-MFSD6

antibody (Sigma Aldrich, Stockholm, Sweden) on the lysates.

Western blot

The cell lysates were mixed with Laemmlis Sample Buffer (Bio-Rad) and 2-mercaptoethanol (Fluka), and loaded onto 12% TGX Miniprotean gels (Bio-Rad) before run at 100 V for 80 min. A pre stained molecular weight marker (Thermo Fischer) was used as a size reference. The proteins were blotted onto a PVDF membrane (Immobilon-P, Millipore) at 4 °C, 50 V for 60 min before blocked for 60 min at RT in 5% nonfat dry milk (Bio-Rad) diluted in 1.5 M NaCl, 0.1 M Tris, 0.05% Tween 20, pH 8.0. Primary antibody anti-MFSD6 (Sigma-Aldrich, Sweden; Goat- SAB2502050; 1:20), was added to the membrane and allowed to bind over night at 4 °C. Then the membrane was washed in TTBS and incubated for 60 min at RT with HRP coupled secondary antibodies (anti-goat (Invitrogen), diluted 1:3000 in milk blocking). The membrane was developed using Clarity Western ECL Substrate (Bio-Rad) and visualised using a CCD camera (Bio-Rad) and staining was compared to the molecular weight marker.

Tissue collection, paraffin embedding and sectioning for protein visualisation

Adult male mice were injected with pentobarbital (0.5 mg/g IP; Apoteksbolaget, Sweden) before transcardiac perfusion was performed by pumping phosphate-buffered saline (PBS) through the left chamber followed by 4% formaldehyde (HistoLab, Sweden). Brains were dissected and stored in 4% formaldehyde overnight followed by post-fixation in zinc-formalin (Richard-Allan Scientific) for 40 min at 40 °C. Brains were then dehydrated in isopropanol (Solveco) and embedded in paraffin (DaLab, Sweden) in a Tissue-Tek vacuum infiltration processor (Miles Scientific). Coronal sections were cut (7 μm) using a Microm 355S STS cool cut microtome and attached on Superfrost Plus slides (Menzel-Gläser, Germany). Each slide was dried overnight at 37 °C and stored at 4 °C.

Fluorescent immunohistochemistry on paraffin embedded sections

Fluorescent immunohistochemistry was performed according to the procedures described in [42], with some modifications. Sections were incubated overnight at 4 °C with the commercial polyclonal antibody anti-MFSD6 (Sigma-Aldrich; Goat- SAB2502050-1:20), anti-MFSD8 (Sigma-Aldrich; Rabbit- HPA044802- 1:50) and anti-MFSD10 (Sigma-Aldrich; Rabbit- HPA037398- 1:20) together with one of the cellular markers Neuronal Nuclei (NeuN), Anti-Glutaminase (PAG) and Anti-Glial Fibrillary Acidic Protein (GFAP) (for antibody information see Table 2), diluted in supermix (Tris-buffered saline, 0.25% gelatin, 0.5% Triton X-100). After 1 h of secondary antibody incubation and DAPI (Sigma-Aldrich, USA; 1:1250) staining, the sections were mounted in Mowiol anti-fade media (25 g Mowiol 4-88 in 100 ml 1xPBS, pH 8.0, 50 ml glycerol, 3 ml of 1% Thimerosal, and 100 μg/ml *n*-propyl gallate in (all from Sigma-Aldrich)). The sections were photographed using a Zeiss AxioPlan 2 fluorescence microscope, connected to an AxioCamHRm camera and the micrographs were finally analysed with Carl Zeiss AxioVision version 4.8 software.

Fluorescent immunocytochemistry on embryonic primary cortex cells

Cortices of embryos (day 14–15) were used to seed primary cell cultures as described in [9]. Pregnant females were euthanised by cervical dislocation for embryo retrieval. Then the samples were dissociated using both chemical and mechanical procedures followed by filtration and single cells were seeded in plating media containing DMEM-F12 (Thermo Fischer Scientific-Gibco), 10% FBS (Thermo Fischer Scientific-Gibco), 2 mM L-glutamine (Thermo Fischer Scientific-Gibco), 1 mM Na-Pyruvate (Thermo Fischer Scientific-Gibco) and 1% penicillin/streptomycin (Thermo Fischer Scientific-Gibco) on poly-L-lysine (Sigma-Aldrich) coated cover slips. The media was changed to growth media containing Neurobasal A (Thermo Fischer Scientific-Gibco), 2 mM L-glutamine (Thermo Fischer Scientific-Gibco), 1 mM Na-Pyruvate (Thermo Fischer Scientific-Gibco) and 1% penicillin/streptomycin (Thermo Fischer Scientific-Gibco) and 2% B27 supplement (Thermo Fischer Scientific-Gibco) after 3 h at 37 °C in presence of 5% CO_2 and the incubation continued under same conditions. 75% of the media was changed every 3–4 days and on day 10 the cells were fixed in 4% formaldehyde for 1 h with several subsequent washes with PBS. Double immunocytochemistry was performed following the standard protocol as described in [9]. The cells were co-stained with anti-MFSD6 and neuronal marker anti-PAN or anti-MFSD6 and lysosomal marker Lamp2 as well as anti-MFSD8 and anti-PAN or anti-MFSD8 and anti-Lamp2 (see Table 2 for antibody concentrations).

Brain collection from food restricted mice for qRT-PCR

To study how altered nutrient intake affected the expression of *Mfsd6*, *Mfsd8* and *Mfsd10* we exposed mice to various food paradigms according to the protocol described in [9]. Briefly, male mice were divided into three groups; 1) controls that were fed standard chow (5% fat, 21% protein, and 51.5% carbohydrates; R3, Lantmännen, Sweden) until dissection ($n = 6$), 2) starved mice that were food deprived for 24 h prior dissection ($n = 4$), and 3) mice with high-fat western diet (consisting of 21% fat by weight, 17.2% protein, 43% carbohydrates; R638, Lantmännen, Sweden) during eight weeks prior dissection to induce obesity ($n = 6$). On the day of dissection, there was a 38% ± 9% increase in weight in the obese group compared to a 12% ± 2.3% increase in controls. All mice had water *ad libitum*. The fresh brains were cut in seven coronal sections using a brain matrix (Alto, 1 mm) according to Figure 7A (adapted from 9] and were placed in RNA-later (Invitrogen) for 2 h followed by RNA extraction and cDNA synthesis as previously described. qRT-PCR was run using the already described primers for *Mfsd6*, *Mfsd8* and *Mfsd10* and the housekeeping genes. The qRT-PCR followed the same conditions as in the RNA panel.

Analysis of qRT-PCR data from mice subjected to different diets

CT-values for all samples were collected and primer efficiency was calculated before correcting the samples accordingly. The GeNorm protocol [41] identified three stable housekeeping genes, *Gapdh*, *H3a* and *Actb*, and their geometric means were used as normalisation factors for each brain section. The CT-values for *Mfsd6*, *Mfsd8* and *Mfsd10* were normalised and plotted (±SD). GraphPad Prism 5 was used for the statistical analyses and charts plotting. Normalised relative mRNA expressions (±SD) were depicted. Unpaired t-tests were run between the controls and the starved group or the HFD group for each brain section, followed by Bonferroni correction for multiple testing; significance levels were set to $^{*}p < 0.0493$, $^{**}p < 0.00998$, $^{***}p < 0.001$.

Disclosure statement

All authors have read and approved the manuscript. The authors declare that they have no conflicts of interest with the contents of this article.

Authors' contributions

SB financed the project, drafted the manuscript, designed experiments and performed part of bioinformatics, immunostainings and microscopy as well as analysis of data.

EP and JL prepared and run the qRT-PCRs. EP analysed the qRT-PCR results and wrote parts of the manuscript. EP prepared the western blot samples and finalised the bioinformatics figures.

KH performed and analysed knocking down experiments with SiRNAs and Western Blots.

NW and SK performed immunostainings.

RF performed part of bioinformatics, financed the project and finalised the manuscript.

Funding

This study was supported by the Swedish Research Council, The Swedish Brain Foundation, The Swedish Society for Medical Research, The Novo Nordisk foundation, Åhlens foundation, Olle Engkvist Byggmästare Foundation, Thurings Foundation for metabolic research, Gunvor and Josef Anérs foundation and Tore Nilssons foundation.

References

[1] Almen MS, Nordstrom KJ, Fredriksson R, et al. Mapping the human membrane proteome: a majority of the human membrane proteins can be classified according to function and evolutionary origin. BMC Biol. 2009;7:50.

[2] Perland E, Fredriksson R. Classification systems of secondary active transporters. Trends Pharmacol Sci. 2017;38(3):305–315.

[3] Hediger MA, Romero MF, Peng JB, et al. The ABCs of solute carriers: physiological, pathological and therapeutic implications of human membrane transport proteinsIntroduction. Pflugers Arch. 2004;447(5):465–468.

[4] Hoglund PJ, Nordstrom KJ, Schioth HB, et al. The solute carrier families have a remarkably long evolutionary history with the majority of the human families present before divergence of Bilaterian species. Mol Biol Evol. 2011;28(4):1531–1541.

[5] Marger MD, Saier MH. Jr. A major superfamily of transmembrane facilitators that catalyse uniport, symport and antiport. Trends Biochem Sci. 1993;18(1):13–20.

[6] Saier MH, Jr., Beatty JT, Goffeau A, et al. The major facilitator superfamily. J Mol Microbiol Biotechnol. 1999;1(2):257–279.

[7] Pao SS, Paulsen IT, Saier MH. Jr. Major facilitator superfamily. Microbiol Mol Biol Rev. 1998;62(1):1–34.

[8] Sreedharan S, Stephansson O, Schioth HB, et al. Long evolutionary conservation and considerable tissue specificity of several atypical solute carrier transporters. Gene. 2011;478(1–2):11–18.

[9] Perland E, Lekholm E, Eriksson MM, et al. The Putative SLC transporters Mfsd5 and Mfsd11 are abundantly expressed in the mouse brain and have a potential role in energy homeostasis. PLoS One. 2016;11(6):e0156912.

[10] Perland E, Hellsten SV, Lekholm E, et al. The Novel Membrane-Bound Proteins MFSD1 and MFSD3 are Putative SLC transporters affected by altered nutrient intake. J Mol Neurosci. 2017;61(2):199–214.
[11] Law CJ, Maloney PC, Wang DN. Ins and outs of major facilitator superfamily antiporters. Annu Rev Microbiol. 2008;62(1):289–305.
[12] Reddy VS, Shlykov MA, Castillo R, et al. The major facilitator superfamily (MFS) revisited. FEBS J. 2012; 279(11):2022–2035.
[13] Fredriksson R, Nordstrom KJ, Stephansson O, et al. The solute carrier (SLC) complement of the human genome: phylogenetic classification reveals four major families. FEBS Lett. 2008;582(27):3811–3816.
[14] Perland E, Bagchi S, Klaesson A, et al. Characteristics of 29 novel atypical solute carriers of major facilitator superfamily type: evolutionary conservation, predicted structure and neuronal co-expression. Open Biol. 2017;7:170142.
[15] Siintola E, Topcu M, Aula N, et al. The novel neuronal ceroid lipofuscinosis gene MFSD8 encodes a putative lysosomal transporter. Am J Hum Genet. 2007;81(1): 136–146.
[16] Damme M, Brandenstein L, Fehr S, et al. Gene disruption of Mfsd8 in mice provides the first animal model for CLN7 disease. Neurobiol Dis. 2014;65:12–24.
[17] Brandenstein L, Schweizer M, Sedlacik J, et al. Lysosomal dysfunction and impaired autophagy in a novel mouse model deficient for the lysosomal membrane protein Cln7. Hum Mol Genet. 2016;25(4): 777–791.
[18] Ushijima H, Hiasa M, Namba T, et al. Expression and function of TETRAN, a new type of membrane transporter. Biochem Biophys Res Commun. 2008;374(2): 325–330.
[19] Mima S, Ushijima H, Hwang HJ, et al. Identification of the TPO1 gene in yeast, and its human orthologue TETRAN, which cause resistance to NSAIDs. FEBS Lett. 2007;581(7):1457–1463.
[20] Lekholm E, Perland E, Eriksson M, et al. Putative membrane-bound transporters MFSD14A and MFSD14B are neuronal and affected by nutrient availability. Front Mol Neurosci. 2017;10. DOI:10.3389/ fnmol.2017.00011
[21] Angers M, Uldry M, Kong D, et al. Mfsd2a encodes a novel major facilitator superfamily domain-containing protein highly induced in brown adipose tissue during fasting and adaptive thermogenesis. Biochem J. 2008;416(3):347–355.
[22] Berger JH, Charron MJ, Silver DL. Major facilitator superfamily domain-containing protein 2a (MFSD2A) has roles in body growth, motor function, and lipid metabolism. PLoS One. 2012;7(11):e50629.
[23] Huang Q, Vera Delgado JM, Seni Pinoargote OD, et al. Molecular evolution of the Slc15 family and its response to waterborne copper and mercury exposure in tilapia. Aquat Toxicol. 2015;163:140–147.
[24] Omasits U, Ahrens CH, Muller S, et al. Protter: interactive protein feature visualization and integration with experimental proteomic data. Bioinformatics. 2014;30(6):884–886.
[25] Biasini M, Bienert S, Waterhouse A, et al. SWISS-MODEL: modelling protein tertiary and quaternary structure using evolutionary information. Nucleic Acids Res. 2014;42(Web Server issue):W252–8.
[26] Jiang D, Zhao Y, Wang X, et al. Structure of the YajR transporter suggests a transport mechanism based on the conserved motif A. Proc Natl Acad Sci USA. 2013; 110(36):14664–14669.
[27] Mullen RJ, Buck CR, Smith AM. NeuN, a neuronal specific nuclear protein in vertebrates. Development. 1992;116(1):201–211.
[28] Manns ID, Mainville L, Jones BE. Evidence for glutamate, in addition to acetylcholine and GABA, neurotransmitter synthesis in basal forebrain neurons projecting to the entorhinal cortex. Neurosci. 2001; 107(2):249–263.
[29] Van der Gucht E, Jacobs S, Kaneko T, et al. Distribution and morphological characterization of phosphate-activated glutaminase-immunoreactive neurons in cat visual cortex. Brain Res. 2003;988(1–2):29–42.
[30] Reeves SA, Helman LJ, Allison A, et al. Molecular cloning and primary structure of human glial fibrillary acidic protein. Proc Natl Acad Sci USA. 1989;86(13): 5178–5182.
[31] Chen JW, Murphy TL, Willingham MC, et al. Identification of two lysosomal membrane glycoproteins. J Cell Biol. 1985;101(1):85–95.
[32] Yu L, McPhee CK, Zheng L, et al. Termination of autophagy and reformation of lysosomes regulated by mTOR. Nature. 2010;465(7300):942–946.
[33] Jones CB, Ott EM, Keener JM, et al. Regulation of membrane protein degradation by starvation-response pathways. Traffic. 2012;13(3):468–482.
[34] Collins S, Martin TL, Surwit RS, et al. Genetic vulnerability to diet-induced obesity in the C57BL/6J mouse: physiological and molecular characteristics. Physiol Behav. 2004;81(2):243–248.
[35] Cunningham F, Amode MR, Barrell D, et al. Ensembl 2015. Nucleic Acids Res. 2015;43(Database issue):D662–9.
[36] Huelsenbeck JP, Ronquist F. MRBAYES: Bayesian inference of phylogenetic trees. Bioinformatics. 2001;17(8):754–755.
[37] Ronquist F, Teslenko M, van der Mark P, et al. MrBayes 3.2: efficient Bayesian phylogenetic inference and model choice across a large model space. Syst Biol. 2012;61(3):539–542.
[38] Notredame C, Higgins DG, Heringa J. T-Coffee: A novel method for fast and accurate multiple sequence alignment. J Mol Biol. 2000;302(1):205–217.
[39] Yan N. Structural biology of the major facilitator superfamily transporters. Annu Rev Biophys. 2015;44: 257–283.
[40] Guex N, Peitsch MC. SWISS-MODEL and the Swiss-PdbViewer: an environment for comparative protein modeling. Electrophoresis. 1997;18(15):2714–2723.
[41] Vandesompele J, De Preter K, Pattyn F, et al. Accurate normalization of real-time quantitative RT-PCR data by geometric averaging of multiple internal control genes. Genome Biol. 2002;3(7):RESEARCH0034.
[42] Hagglund MG, Sreedharan S, Nilsson VC, et al. Identification of SLC38A7 (SNAT7) protein as a glutamine transporter expressed in neurons. J Biol Chem. 2011;286(23):20500–20511.